Analysis of Single Event Transients in Arbitrary Waveforms Using Statistical Window Analysis

J. L. Carpenter, *Member, IEEE*, T. N. Peyton, *Student Member, IEEE*, B. R. Dean, *Student Member, IEEE*, S. P. Lawrence, *Student Member, IEEE*, R. D. Young, *Student Member, IEEE*, D. R. Reising, *Senior Member, IEEE*, and T. D. Loveless, *Senior Member, IEEE*

***Abstract*— Window or taper functions are commonly used in data processing to detect transient events or for time-averaging of frequency spectra. A generalized window function is demonstrated using the ionizing radiation effects spectroscopy (IRES) technique to enhance the measurement of transient anomalies within arbitrary waveforms. The IRES filter is used to convolve time data with a sliding window consisting of a moment-generating function. The resulting time-dependent statistical moments can be used to eliminate any steady-state signatures, including noise, and extract transient behaviors. The IRES filter is used to analyze data from heavy-ion exposures of commercial off-the-shelf (COTS) operational amplifiers (Op-Amps), laser-induced transients in CMOS phase-locked loops (PLLs), and simulated transients in digital and analog circuits. The performance of the IRES filter in noisy environments shows that transients can be measured with higher fidelity than standard amplitude thresholding. This statistical window analysis technique may remove the need for complex triggering mechanisms on instrumentation and does not require a priori knowledge of transient characteristics. Potential applications of IRES include real-time measurement, in situ data analysis, and machine learning (ML).**

***Index Terms*— Analog, digital, ionizing radiation effects spectroscopy (IRES), operational amplifier (Op-Amp), radiation effects, single-event effects, single-event transients (SETs), spectroscopy, time–frequency analysis.**

I. Introduction

THE growing commercialization of space has increased the demand for accelerated ground-based radiation testing facilities. Furthermore, the use of commercial off-the-shelf (COTS) components, systems-on-chip (SoC), and heterogeneous packaged parts often require additional time, specialized facilities, or extensive preparation (such as package de-lidding) before experimentation. Therefore, techniques for improving the automation of radiation testing and data collection and analysis are critical for meeting the growing constraints.

Previous works introduced ionizing radiation effects spectroscopy (IRES) for in situ analysis of total ionizing dose (TID) degradation [1] and single event transients (SETs) in RF circuits [2], [3]. The IRES leverages time–frequency domain analysis techniques common in data communications [4], [5] for identifying anomalous behavior by "imaging" the statistical features of a waveform. However, all previous studies that leverage IRES use clock signals from an RF phase-locked-loop (PLL) circuit [1], [2], [3]. In addition, these studies all paired IRES with machine learning (ML) for the study and classification of the results. This article generalizes the IRES methodology, proposing the IRES window filter that uses a statistical moment generating function for detecting and characterizing anomalous behavior within arbitrary waveforms, such as those found in steady-state digital, steady-state dc, steady-state ac, and RF applications. Specifically, the sensitivities of some of the primary moments to radiation-induced transients are illustrated. Possible algorithms, including ML-based solutions, for using one or more of the moment-based features are discussed and compared with standard instrumentation thresholding techniques.

Transient data were collected from heavy-ion exposures at the Lawrence Berkeley National Laboratory (LBNL) 88″ Cyclotron, Michigan State University's (MSU) Facility for Rare Isotope Beams (FRIB) linear accelerator, and from experiments at the Naval Research Laboratory's (NRL) Two-Photon Absorption (TPA) laser [6], [7]. Devices under test (DUT) include COTS LM124 Operational Amplifiers (Op-Amp) and custom PLL sub-circuits fabricated in a CMOS 130 nm technology [8]. In addition, fault injection experiments on an 8-bit digital-to-analog converter (DAC) illustrate the ability to detect single event upsets (SEUs) in a digital sequence.

Measured data show that the IRES window filter enhances transient analysis by eliminating all steady-state signatures, including continuous noise, and extracts transient behaviors by amplifying shifts in statistical moments. Furthermore, the performance of the IRES filter in noisy environments shows that a single IRES filter can reduce the signal-to-noise ratio (SNR) requirement for detection by over 10 dB, and sequential IRES filters can improve the response by over 20 dB when compared with traditional threshold triggers. In addition, while threshold triggers require a positive-valued SNR, IRES is shown effective even with SNR values as low as −17 dB, detecting anomalies in high noise environments without requiring multi-sampling. Finally, IRES is highly effective in extracting transients within ac waveforms,

Manuscript received 3 January 2023; revised 1 February 2023; accepted 3 February 2023. Date of publication 9 February 2023; date of current version 18 April 2023. This work was supported in part by the Defense Threat Reduction Agency under Award HDTRA1-17-1-0003.

The authors are with the Electrical Engineering Department, University of Tennessee at Chattanooga, Chattanooga, TN 37403 USA (e-mail: rdt249@mocs.utc.edu).

Color versions of one or more figures in this article are available at https://doi.org/10.1109/TNS.2023.3243496.

Digital Object Identifier 10.1109/TNS.2023.3243496

such as clock signals, without requiring prior signal transformations.

II. Analysis of SETs With IRES

The SETs result from the interaction of ionizing radiation with sensitive junctions in integrated circuits (ICs). SETs, which manifest as temporary, random, and unwanted signal transitions, can be mitigated through hardware manipulation, such as filtering or redundancy, at the cost of increased area and power and decreased bandwidth [9]. However, effective radiation-hardening-by-design (RHBD) generally requires detailed knowledge of how the erroneous charge can change the observable behavior at the output of a device. Typically, a test engineer will design an experiment to detect such anomalous behavior by determining a threshold error in voltage or current to trigger measurement hardware. This approach always presents a risk of missing unexpected erroneous behavior and is always based on the noise constraints imposed by the measurement system. Unfortunately, heavy ion test facilities are extremely noisy environments that can inject artificial noise into the system. Transients will not be detected if they occur below the noise level set in the triggering hardware. The IRES detects SET signatures in arbitrary signals, including digital data buses, analog dc and sinusoidal waveforms, and RF signals, without defining an arbitrary error threshold. The statistical windowing technique builds a model of the circuit behavior. Thus, any erroneous behavior can be identified in situ, allowing for further analysis by a radiation test engineer or through ML as published in [3].

A. IRES Window Filter

The IRES is based on radio frequency-distinct native attributes (RF-DNAs) fingerprinting methodologies and signal processing techniques [10], [11], [12], [13], [14], [15], [16], [17], [18], [19], [20]. RF-DNA is used in wireless communication applications to augment security protocols by basing authenticity requirements on statistical features derived from transmitted waveforms. Features are associated with intrinsic variability within the system and are often measured via short-time domain statistical behavior. The IRES extracts stochastic features of a waveform and uses the resulting profiles for a statistics-based assessment of transient behavior. The presence of a transient is determined based on the likelihood that a sampled behavior is statistically different from expected steady-state behavior.

A diagram of the general methodology is shown in Fig. 1, where an arbitrary discrete time-domain waveform or data sequence is analyzed by viewing smaller "windowed" segments and sliding the viewing window throughout the waveform. This work uses a window function for computing the statistical moments to develop time-dependent statistical profiles. The window function can include features from any signal metric in the time or frequency domain. Furthermore, the window function may be applied concurrently or sequentially with additional windowing functions.

The proposed IRES window filter is used to convolve measured data with a statistical moment-generating function

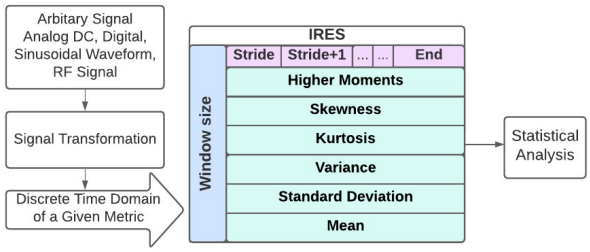

Fig. 1. Block diagram of the IRES methodology where an arbitrary time-domain waveform or data sequence is analyzed by viewing smaller "windowed" segments and sliding the viewing window throughout the waveform. A statistical profile is developed with respect to time and can include features from any signal metric in the time or frequency domain.

through a sliding window. As a result, any number of statistical moments describing nuanced features of data contained within a given window can be computed. Given time-domain data within a window, represented as a random variable X, the kth moment of a random variable X is defined to be the expectation of X^k, or $E(X^k)$. Likewise, the kth central moment of a random variable X is defined to be $E((X - E(X))^k)$. For example, the first moment can be computed by determining the expectation of X and is defined as the mean (μ), whereas the second central moment is defined as the variance (σ^2). Rather than deriving expressions for the individual moments, a moment-generating function, M_{X_i}, can be used to compute all moments of X. Equation (1) represents the moment generating function for X_i, the data consisting of the N time samples within the ith window and consisting of real-valued numbers t. In other words, M is determined as the expectation of the random variable e^{tX_i}

$$M_{X_i}(t) = E\left(e^{tX_i}\right). \tag{1}$$

For a discrete and windowed data set, M can be reduced to (2), where $P_i(x)$ is the probability mass function (PMF) of X_i

$$M_{X_i}(t) = \sum_{X_i} e^{tx} P_i(x). \tag{2}$$

It follows that M can then be used to derive up to k moments of X_i using (3), where the kth derivative of M with respect to t is computed and evaluated at $t = 0$. Thus, any number of moments $E(X^k)$ can be computed within each discrete window and appended to form an IRES spectrogram as described in [2]

$$E\left(X^k\right) = \frac{d^k}{dt^k} M_{X_i}(t)\bigg|_{t=0}. \tag{3}$$

The first four moments (i.e., mean μ, variance σ^2, skewness γ, and kurtosis κ) are described in [2]. μ is useful for identifying the worst case deviation of the signal, whereas σ^2 or σ measures emphasize the sharpness of a transition within the signal. γ and κ are measures indicating an abrupt transition from steady-state (i.e., the start, recovery, or ending of a transient anomaly). Here, the sixth and seventh moments are also used, representing smoothed versions of γ and κ, respectively. The sixth and seventh moments may be used in

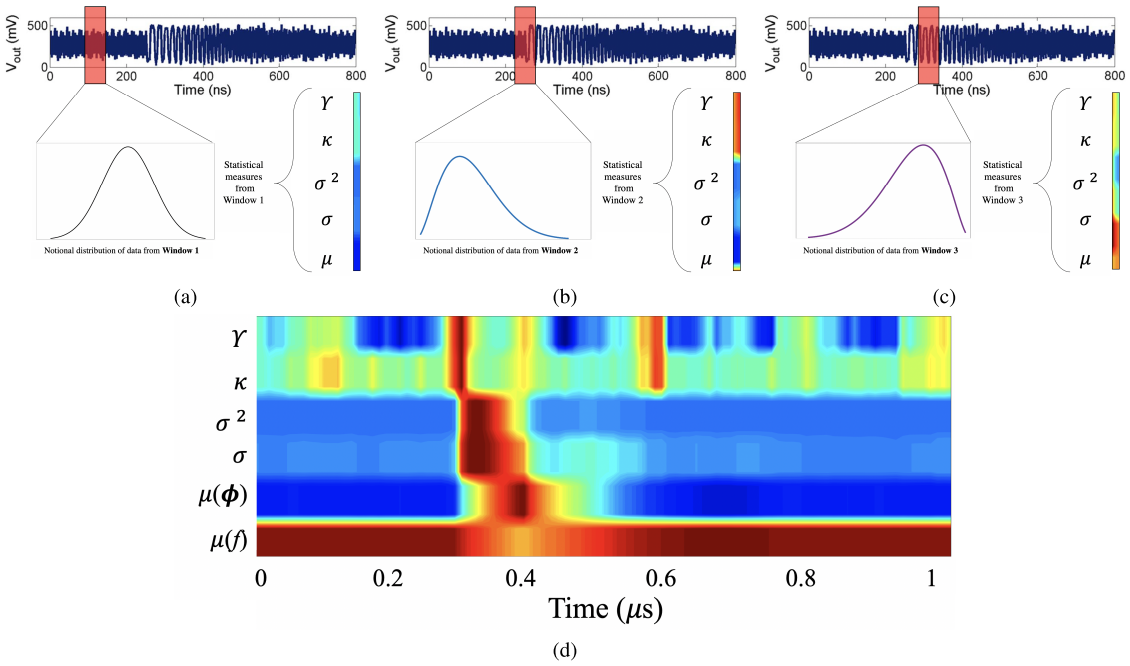

Fig. 2. Example IRES spectrogram (d) for visualizing various statistical moments of a signal's behavior (a) pre-, (b) during, and (c) post-strike. Probability density functions are estimated within the sliding windows, and several statistical moments are calculated. Here, the time evolution of the mean of the signal's frequency [$\mu(f)$], the mean of the signal's phase [$\mu(\phi)$], the variance (σ^2), standard deviation (σ), kurtosis (κ) and skewness (γ) of the phase are illustrated (after [3]).

identifying the presence of an anomaly through more discrete indicators of a disruption.

An advantage of the IRES moment-generating filter is the ability to process arbitrary (i.e., the signal type is irrelevant) discrete waveforms. The resulting statistical moments can aid in detecting abnormalities caused by SETs, improving measurement fidelity, especially in noisy environments. An example is shown in Fig. 2, where time-sequenced moments of a clock signal's frequency and phase are used to develop and visualize the shifting statistical profiles before, during, and after the presence of an SET. In Fig. 2, a clock signal's behavior [Fig. 2(a)] pre-, [Fig. 2(b)] during, and [Fig. 2(c)] post-strike are visualized after applying IRES window filters and normalizing each moment to the maximum value in each field. PMFs are estimated within the sliding windows, and several statistical moments are calculated. Here, the time evolution of the mean of the signal's frequency [$\mu(f)$], the mean of the signal's phase [$\mu(\phi)$], and σ^2, σ, κ, and γ of the phase are illustrated following a perturbation by an ion [3].

B. Devices Under Test

IRES was applied to various analog, digital, and RF DUTs. First, the LM124 Op-Amp was chosen to represent a ubiquitous and well-characterized analog component [21], [22]. In addition, a custom synthesized 8-bit DAC, realized using the Python programming language, is used to demonstrate IRES for extracting SEUs within a digital signal. Finally, a custom PLL fabricated in a CMOS 130 nm technology node is used to illustrate the use of IRES in RF and clock waveforms [8]. Results obtained from a standard amplitude thresholding methodology are compared with results obtained by thresholding the individual IRES-generated moments to quantify the effectiveness of the statistical moments for SET detection.

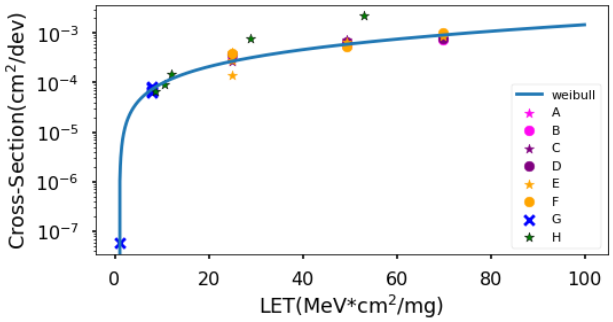

Fig. 3. LM124 SET cross section (cm^2/dev) versus LET (MeV $\times$ cm^2/mg) for data obtained at LBNL and MSU and compared with the reference data "H" represented by green stars obtained at NSRL [23]. Table I details the test configurations.

III. Experimental Setup

A. LM124

The LM124 Op-Amps were irradiated at the LBNL 88″ Cyclotron and the MSU's FRIB linear accelerator. At LBNL, Xe and Kr ions in the 16 MeV/amu cocktail were utilized in air (with the approximate LET values of 49 and 25 MeV $\times$ cm^2/mg, respectively) with fluxes ranging from 4.5×10^3 to 2.0×10^7 ions/cm^2/s. At the MSU's FRIB, 20 MeV/amu Ar and 30.5 MeV/amu O ions were utilized (with the approximate LET values of 7.9 MeV $\times$ $-$cm^2/mg and 1.0 MeV $\times$ cm^2/mg, respectively) with fluxes ranging from

TABLE I
TESTING CONDITIONS

Measurements	Device	Facilities	Configuration	Gain	Bias
A	LM124	LBNL	Inverting	10V/V	0.1V
B	LM124	LBNL	Inverting	10V/V	0.5V
C	LM124	LBNL	Non-Inverting	10V/V	0.1V
D	LM124	LBNL	Non-Inverting	10V/V	0.5V
E	LM124	LBNL	Non-Inverting	1V/V	1V
F	LM124	LBNL	Non-Inverting	1V/V	5V
G	LM124	FRIB(MSU)	Non-Inverting	1V/V	1V
H	LM124	NASA	Non-Inverting	1V/V	1V
I	Mixed-Signal PLL*	NRL			

* The mixed-signal PLL circuit, fabricated in the IBM 130 nm CMRF8RF CMOS technology, is detailed in [8]. The device has a center frequency of 200 MHz and a maximum frequency of 530 MHz. The locking range of the PLL is between 40 and 350 MHz, with a gain of 7.75 GHz/V.

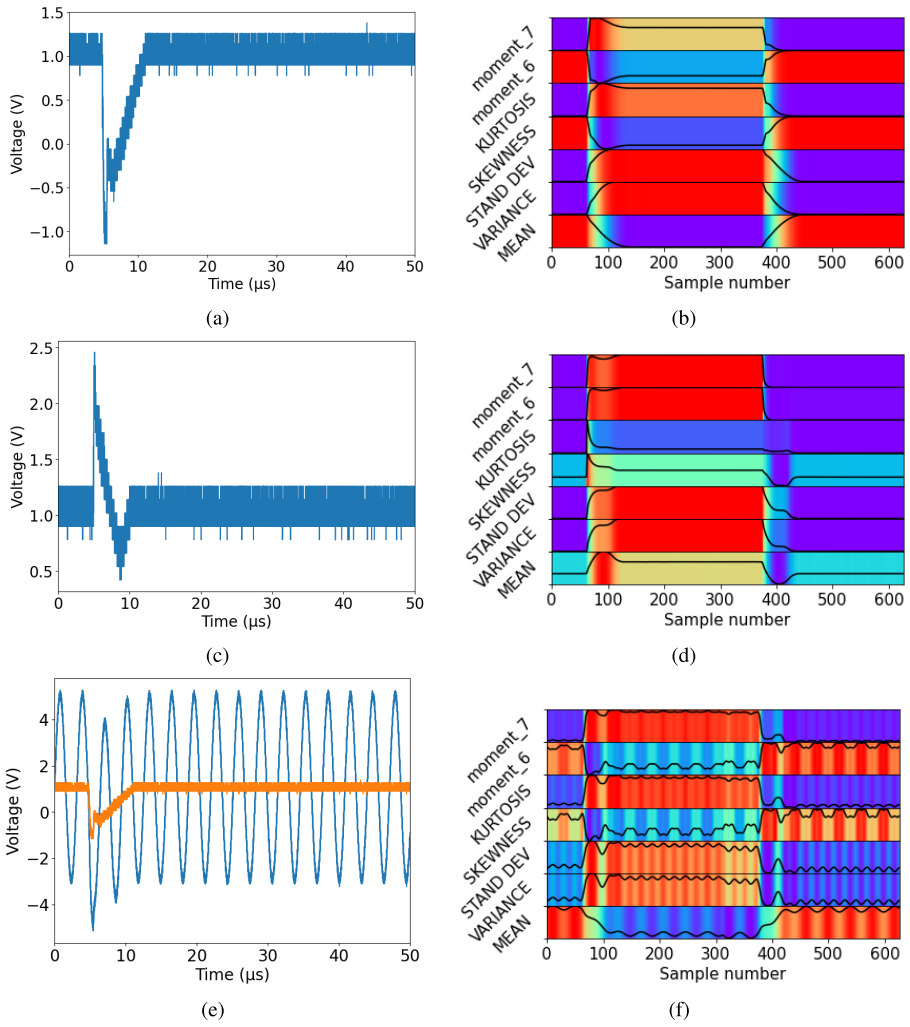

Fig. 4. Analog SETs in the LM124 following exposure to Xe ions (16 MeV/amu) at LBNL. The incident LET was 49.3 MeV × cm^2/mg. The LM124 was configured in unity gain with a dc input of $V_{in} = 1$ V in (a) and (c), and with a sinusoidal input with a dc offset of 1 V and a 8 V amplitude in (e). (b), (d), and (f) Corresponding IRES spectrograms, including the mean, variance, standard deviation, skewness, kurtosis, and the sixth and seventh moments.

4.5×10^3 to 1×10^4 ions/cm^2/s. SRIM [24] was used in all cases to determine the LET at the surface of the de-lidded die.

The LM124 DUTs were tested in inverting and non-inverting configurations having different gains, varying input voltages, and with $V_{DD} = 15$ V and $V_{SS} = -15$ V. Table I details the configurations of each DUT. The angle of incidence was set to either 0° or 45°. Each ion exposure was conducted until 100 SETs were acquired, except for the O ion at the FRIB that was run to a total fluence of 5.16×10^7 ions/cm^2. In this case, the incident LET (of ≈1 MeV × cm^2/mg) was

near the LET threshold of the LM124, and the fluence was chosen to establish a limiting cross section; three SETs were recorded.

The LM124 DUTs were connected to a Tektronix DPO7104 Oscilloscope (Oscope) through coaxial cables and BNC connectors. A window trigger was set to be ±0.5 V above the nominal output voltage, and pre-irradiation measurements were obtained to ensure that no false-positive, noise-induced events were captured. SETs were saved locally to a solid-state drive. A programmable dc power supply was connected by a coaxial cable and a BNC connector to the differential input of the DUT. A second power unit supplied a biasing voltage of ±15 V. The programmable dc power supply and Oscope were connected to a computer through an Ethernet switch. Python script commands were sent from the computer to the testing equipment. After testing, the SET data were evaluated with the IRES analysis software. Fig. 3 shows the SET cross section (cm^2/dev) versus LET (MeV × cm^2/mg) results for the LM124 DUTs irradiated at LBNL and MSU. Data obtained at NSRL from [23], marked by the green stars in Fig. 3, are also included for reference and to show consistent results with the prior literature.

B. CMOS PLL

A custom PLL fabricated in a 130 nm CMOS technology was used to obtain transient data at NRL's TPA facility using a high peak power femtosecond laser at sub-bandgap optical wavelengths [6], [7], [25], [26], [27]. The DUT was mounted on a motorized xyz translation platform with 0.1 μm resolution, and the TPA laser was focused on the PLL's subcircuits. Waveforms were collected at the PLL circuit's output at the resulting ten thousand (10 000) strike locations, allowing for visualization of the 2-D spatial sensitivity. Ten independent measurements were taken at each strike location, amounting to 1 00 000 individual waveforms. Additional details on this dataset can be found in [3] and [8]. This work leverages these data to analyze the effectiveness of the IRES window filter on sinusoidal data in the presence of noise.

IV. Results

A. IRES for Analog Signals

The SETs observed during accelerator testing were the result of excess mobile charge converted from the interaction of ionized particles with the semiconductor material. These anomalies may manifest as spurious voltages that can compete with the nominal signals or become latched as incorrect data in memory. Fig. 4(a) and (c) illustrates the examples of analog SETs captured from an LM124 during a heavy ion radiation test at LBNL. In both cases, the LM124 was configured in a non-inverting, unity-gain configuration (i.e., voltage follower) with a dc input of 1 V. The Xe ion (16 MeV/amu) was utilized with an incident LET of 49.3 MeV × cm^2/mg. Fig. 4(e) illustrates a similar transient with a sinusoidal input where the dc offset was 1 V, and the sinusoidal amplitude was ≈4 V.

Testing is usually conducted under dc conditions, because the transients [as in Fig. 4(a) and (c)] are detectable above a static threshold above the noise level. As seen in Fig. 4(e), ac transients require more complicated instrumentation thresholding techniques. However, IRES can extract the SET signal even when the error response competes with excessive noise or ac signals. IRES allows for the analysis of short-duration transient behavior via time–frequency analysis [2] and filters out the nominal circuit behavior, thus extracting the error signal. Fig. 4(b), (d), and (f) illustrates the IRES spectrograms for the three transients and are constructed using μ, σ, σ^2, κ, γ, and the sixth and seventh moments. The spectrograms are unique to the underlying transient characteristics, as seen by comparing Fig. 4(b) and (d), and are readily obtained from dc or sinusoidal signals as seen by comparing Fig. 4(b) and (f). μ represents an ac-filtered version of the original signal. σ and σ^2 are the measures of the transient time constants, and κ and γ are signal event transitions. As seen in Fig. 4(f), the steady-state ac sinusoidal waveform has a secondary effect on the calculated moments.

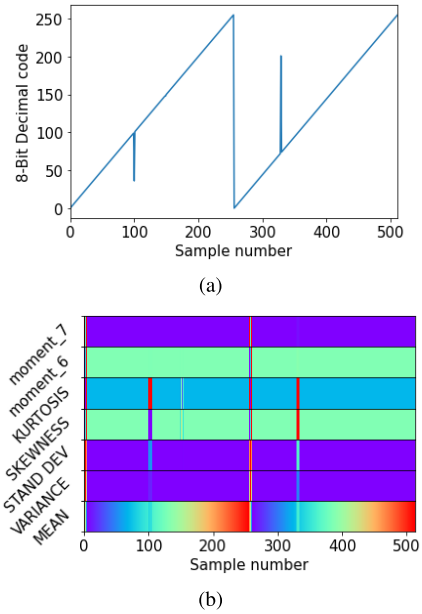

Fig. 5. (a) SEUs in the software DAC with an applied ramp function and (b) associated IRES spectrogram. Two periods of an 8-bit ramp function are visualized with three SEUs injected in random bit locations. Two SEUs are visible in (a) samples 100 and 325. However, small changes in the skewness and kurtosis indicate the presence of an, otherwise, undetectable SEU in sample 150. The changing colors represent the normalized values ranging from 0 (purple) to 1 (red).

The window size for the IRES spectrograms displayed in Fig. 4 was chosen to be 50% of the total number of recorded time steps, and a stride of 800-time steps was used. Here, a window size of 50% corresponds to ≈25 μs. While not necessarily the optimal window size nor stride, the large window size guaranteed that the sliding window would encompass the transients (note that the transient widths in the LM124 are well understood and documented) while also filtering out the steady-state noise. Additional work is required to determine the optimal sliding window parameters to automate SET detection.

B. IRES for Digital Signals

1) Deterministic Digital Signals: An 8-bit software DAC and a fault injection tool were developed using Python to

accept a discrete-time sequence of 8-bit digital data and convert it to an analog signal for analysis with the IRES module. Fig. 5(a) illustrates the 8-bit decimal code with an applied ramp function (counting from 0x00 to 0xFF). Faults (SEUs) were injected by randomly selecting one of eight bits during a random sample out of signal. The SEUs can be seen as positive or negative spikes in the digital ramp signal, having different amplitudes based on which bit was flipped: two are distinct, because the SEUs occurred in the most significant bits, whereas one SEU is not visible at scale, because it occurred in the least significant bit (LSB). However, when IRES is applied to the digital waveform, shown in Fig. 5(b), small changes in κ and γ appear at $\approx$150 cycles (sample number), indicating the, otherwise, undetectable presence of the SEU. The two most significant features for the digital data appear to be κ and γ, as they represent coarse data transitions. The window size for the IRES spectrogram was set to five time steps with a stride of one step. The changing colors represent the normalized values ranging from 0 (purple) to 1 (red). Note that the IRES algorithm does not require a golden sample of the unperturbed data sequence, as it establishes probabilities of upset based on prior functionality. Although a DAC with an applied ramp function was used to illustrate the implementation of IRES with binary (base-2) signals, the technique can be applied to any digital code as long as the window is larger than the number of bits required to represent the base-2 numbers.

2) Stochastic Digital Signals: Signals with low entropy (such as a ramp function or other deterministic digital data) are straightforward to analyze; however, stochastic data with high entropy present a challenge for the technique. When a signal is stochastic, such as in digital communication signals, and has a high entropy factor, the IRES methodology loses its effectiveness. One way of detecting SEUs in digital stochastic signals could be through double transmission. IRES can compare the two signal PMFs and find the accrued error using temporally or spatially redundant information, but further work is needed for validation.

C. IRES Noise Sensitivity

The IRES window filter is naturally robust to noisy signals, as the method extracts transient phenomena based on probabilities. Therefore, a comparison between a typical thresholding technique (a priori determination of signal boundaries, typically based on maximum and minimum levels of acceptable voltage/current) and the IRES method was conducted. First, the PLL dataset, including 1 00 000 transient measurements induced by the TPA laser at NRL, was used to evaluate the sensitivity of IRES with varying window settings and under varying noise constraints. These measured data include ten samples for each location where an SET was injected. These data were augmented by adding artificial random white Gaussian noise (WGN) to the original waveform data, resulting in SNR values ranging from 0 to 13.01 dB. The SNR was calculated by (4), where μ is the mean of the expected signal power of the raw data, and σ is the standard deviation of the WGN. To convert SNR to decibels, (5) is used. The ten unique signals (corresponding to identical locations in the PLL) were

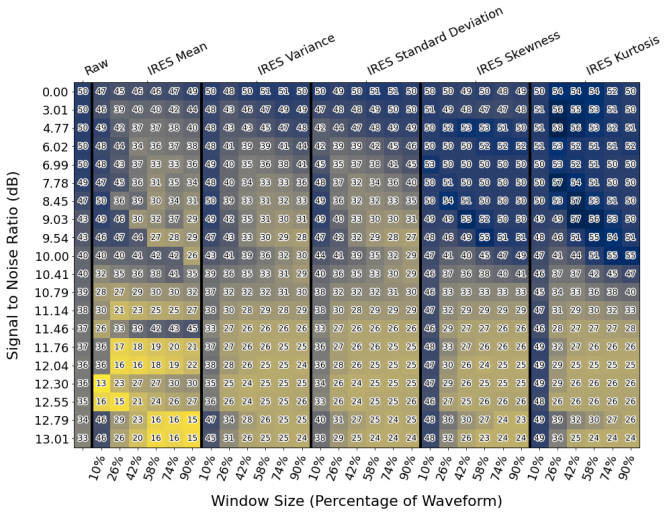

Fig. 6. Comparison of error thresholding a raw waveform against IRES-generated moments with different window filter sizes. The Y axis represents the SNR, and the bottom X axis portion represents the window size of the IRES filter (in units % of time steps). The top X axis portion indicates the waveform or time-sequenced moment that was evaluated, separated by the vertical lines.

each evaluated with a different WGN profile at the same SNR value

$$\text{SNR} = \frac{\mu}{\sigma} \tag{4}$$

$$\text{SNR}_{\text{dB}} = 10\log_{10}(\text{SNR}). \tag{5}$$

Each augmented, noisy waveform consists of 500 time steps. First, a baseline threshold method was defined; in this case, μ and σ of 100 random waveforms were measured. Next, SETs were defined if any point within a sample fell outside of three standard deviations from the mean. This process was repeated for all SNR values.

In addition, each waveform was transformed using window IRES filters with varying window sizes (ranging from 10% of the time steps to 90% of the time steps) and a fixed stride of 10%. Similar to the baseline amplitude thresholding method, the sensitivity of the individual moments to WGN was evaluated by defining an SET when any point within a sample fell outside of three standard deviations from the mean of the moment under study. This process was repeated for all SNR values. The percentage error was used to compare the results and is determined by (6). True positive (TP) represents the number of times a waveform was correctly identified as containing an SET; true negative (TN) represents the number of correctly identified waveforms without an SET; false positive (FP) represents the number of incorrectly identified transients; false negative (FN) represents the number of waveforms incorrectly identified as unperturbed. Note that this process was conducted to examine the sensitivity of each IRES-generated moment to the transient signal and is not intended to suggest an SET detection process. An IRES-inspired SET detection process will likely involve a combination of moments and ML-based classification

$$\text{Error} = \frac{\text{FN} + \text{FP}}{\text{TN} + \text{TP} + \text{FN} + \text{FP}}. \tag{6}$$

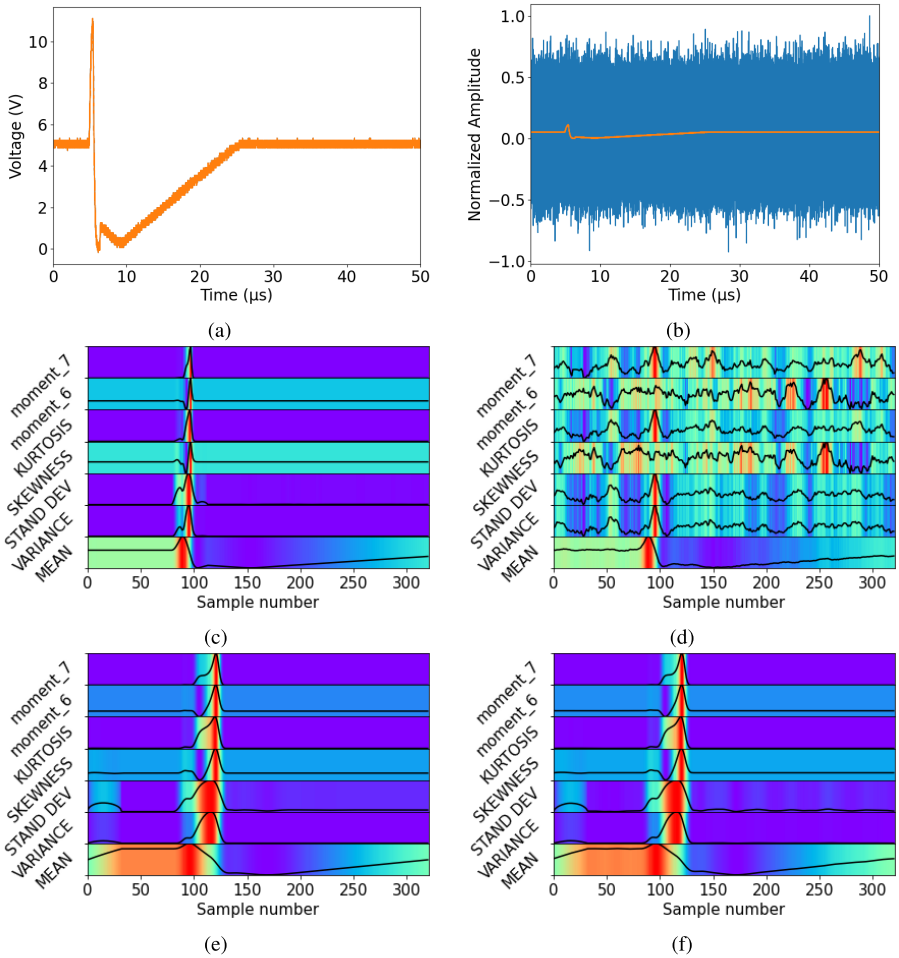

Fig. 7. Analog SETs in the LM124 following exposure to Xe ions (16 MeV/amu) at LBNL. The incident LET was 49.3 MeV × cm^2/mg. (a) LM124 was configured in unity gain with a dc input of $V_{\text{in}} = 5$ V. (b) LM124 was configured in unity gain with a dc input of $V_{\text{in}} = 5$ V with random WGN added to the transient for an SNR of −17 dB. (c) and (d) Corresponding spectrograms following one application of the IRES filter (IRES$_1$). (e) and (f) Corresponding spectrograms following two sequential applications of the IRES filter (IRES$_2$). Both IRES$_1$ and IRES$_2$ spectrograms include the mean, variance, standard deviation, skewness, kurtosis, and the sixth and seventh moments.

Fig. 6 shows the percentage error of a chosen threshold metric (i.e., the original, raw waveform versus various IRES-generated moments) with respect to window size and SNR. The color corresponds to the error value of each cell. First, the baseline thresholding technique resulted in a minimum error of 31% for an SNR of 13 dB. The method cannot tolerate high levels of noise without defining new metrics. Moreover, transients that exist within the noise boundaries are not detectable. The first and second moments outperform the baseline technique, with μ as perhaps the most reliable single metric for identifying the presence of a transient. The lowest error rate is observed at a window size of 26%; however, larger window sizes appear to improve the performance for critically low SNR values. In other words, while small window sizes can be useful for detecting fast transients, calculations will be more sensitive to noise when compared with large window sizes. The third moments and higher are susceptible to noise and cannot be used for transient thresholding except in cases with large SNR values. The percentage error generally increases with decreasing SNR for all moments, though the SNR value at which the percentage error saturates increases with increasing moment. There are trade-offs in accuracy and precision when implementing the IRES window filter. For example, large window sizes improve tolerance to noise at the sacrifice of precision, whereas smaller window sizes improve accuracy while less effective in filtering noise.

While Fig. 6 is intended to show the sensitivity of a single IRES-generated moment to noise and various filter settings, IRES is most beneficial, because several time-sequenced moments are generated simultaneously. In this case, an algorithm is required to leverage more than one moment for thresholding an event detector. Nevertheless, the transient nature of the moments can help develop a more complete understanding of the transient phenomena, be used to build a new definition of a transient threshold, or be used in ML applications and classification models, such as [3].

In addition, IRES window filters may be applied in sequence. Fig. 7(a) shows an example analog SET measured at the output of the LM124 following exposure to Xe ions (16 MeV/amu) at LBNL. The incident LET was 49.3 MeV × cm^2/mg. The LM124 was configured in unity gain with a dc input of $V_{\text{in}} = 5$ V. Fig. 7(b) shows the

identical transient with added WGN to reduce the SNR to −17 dB. Two passes of the IRES window filter were applied to these data. $IRES_1$ corresponds to the output of the first IRES window filter, and $IRES_2$ corresponds to the output of the second IRES window filter in sequence. Since μ of $IRES_1$ was identified as the most informative according to Fig. 6, μ from $IRES_1$ was fed back into the IRES algorithm to produce the spectrograms shown in Fig. 7(e) and (f). A similar process could be conducted using the other moments. The identical spectrograms in Fig. 7(e) and (f) show that the IRES is highly effective in removing high levels of noise, allowing for the extraction of the true transient error signals with high accuracy.

V. Conclusion

This article describes a generalized methodology for using IRES window filters to detect SET signatures in arbitrary dc, periodic, digital, and RF signals. The statistical window analysis technique generates time-sequenced moments of a waveform. These time-dependent moments can be used to describe the transient characteristics beyond the typical amplitude and time-width parameters and may be used to replace or augment typical amplitude based triggering mechanisms. Data collected from heavy-ion exposure of the LM124 at the LBNL 88″ Cyclotron and MSU's FRIB demonstrate the IRES methodology for analog dc, sinusoidal signatures, and noise sensitivity. Fault injection simulations of an 8-bit software DAC are used to illustrate the use of IRES for digital SEU detection. Finally, data from laser TPA experiments on a custom CMOS PLL circuit are used to examine the sensitivity of the IRES-generated moments to noise. IRES outperformed the standard thresholding method by effectively identifying SETs in excessive SNRs. IRES has applications in real-time measurement, in situ data analysis, and ML.

Acknowledgment

The authors would like to thank G. Allen and the team at the JPL, T. Turflinger, K. Label, M. Campola, and the team at the NASA GSFC, J. Caulkins, and the Michigan State University's (MSU) Facility for Rare Isotope Beams (FRIB) Team for aiding in the testing at the MSU's FRIB Facility.

References

[1] B. Patel et al., "Ionizing radiation effects spectroscopy for analysis of total-ionizing dose degradation in RF circuits," *IEEE Trans. Nucl. Sci.*, vol. 66, no. 1, pp. 61–68, Jan. 2019.

[2] T. D. Loveless et al., "Ionizing radiation effects spectroscopy for analysis of single-event transients," *IEEE Trans. Nucl. Sci.*, vol. 67, no. 1, pp. 99–107, Jan. 2020.

[3] T. D. Loveless, D. R. Reising, J. C. Cancelleri, L. W. Massengill, and D. Mcmorrow, "Analysis of single-event transients (SETs) using machine learning (ML) and ionizing radiation effects spectroscopy (IRES)," *IEEE Trans. Nucl. Sci.*, vol. 68, no. 8, pp. 1600–1606, Aug. 2021.

[4] D. R. Reising, M. A. Temple, and M. J. Mendenhall, "Improving intra-cellular security using air monitoring with RF fingerprints," in *Proc. IEEE Wireless Commun. Netw. Conf.*, Apr. 2010, pp. 888–893.

[5] D. Reising, J. Cancelleri, T. D. Loveless, F. Kandah, and A. Skjellum, "Radio identity verification-based IoT security using RF-DNA fingerprints and SVM," *IEEE Internet Things J.*, vol. 8, no. 10, pp. 8356–8371, May 2021.

[6] D. McMorrow, W. T. Lotshaw, J. S. Melinger, S. Buchner, and R. L. Pease, "Subbandgap laser-induced single event effects: Carrier generation via two-photon absorption," *IEEE Trans. Nucl. Sci.*, vol. 49, no. 6, pp. 3002–3008, Dec. 2002.

[7] D. McMorrow et al., "Three-dimensional mapping of single-event effects using two photon absorption," *IEEE Trans. Nucl. Sci.*, vol. 50, no. 6, pp. 2199–2207, Dec. 2003.

[8] T. D. Loveless, L. W. Massengill, W. T. Holman, B. L. Bhuva, D. McMorrow, and J. H. Warner, "A generalized linear model for single event transient propagation in phase-locked loops," *IEEE Trans. Nucl. Sci.*, vol. 57, no. 5, pp. 2933–2947, Oct. 2010.

[9] T. D. Loveless, "Hardening techniques for analog and mixed-signal circuits," in *Proc. IEEE NSREC Short Course*, Jul. 2021, pp. III.1–III.96.

[10] D. R. Reising, M. A. Temple, and J. A. Jackson, "Authorized and rogue device discrimination using dimensionally reduced RF-DNA fingerprints," *IEEE Trans. Inf. Forensics Security*, vol. 10, no. 6, pp. 1180–1192, Jun. 2015.

[11] L. Xiao, L. Greenstein, N. Mandayam, and W. Trappe, "Fingerprints in the ether: Using the physical layer for wireless authentication," in *Proc. IEEE Int. Conf. Commun.*, Jun. 2007, pp. 4646–4651.

[12] B. Kroon, S. Bergin, I. O. Kennedy, and G. O. Zamora, "Steady state RF fingerprinting for identity verification: One class classifier versus customized ensemble," in *Artificial Intelligence and Cognitive Science*, L. Coyle and J. Freyne, Eds. Berlin, Germany: Springer, 2010, pp. 198–206.

[13] C. K. Dubendorfer, B. W. Ramsey, and M. A. Temple, "An RF-DNA verification process for ZigBee networks," in *Proc. IEEE Mil. Commun. Conf. (MILCOM)*, Oct./Nov. 2012, pp. 1–6.

[14] D. R. Reising and M. A. Temple, "WiMAX mobile subscriber verification using Gabor-based RF-DNA fingerprints," in *Proc. IEEE Int. Conf. Commun. (ICC)*, Jun. 2012, pp. 1005–1010.

[15] D. R. Reising, "Exploitation of RF-DNA for device classification and verification using GRLVQI processing," Ph.D. dissertation, Air Force Inst. Technol., Wright-Patterson AFB, OH, USA, Dec. 2012.

[16] W. Wang, Z. Sun, S. Piao, B. Zhu, and K. Ren, "Wireless physical-layer identification: Modeling and validation," *IEEE Trans. Inf. Forensics Security*, vol. 11, no. 9, pp. 2091–2106, Sep. 2016.

[17] G. Baldini, R. Giuliani, and G. Steri, "Physical layer authentication and identification of wireless devices using the synchrosqueezing transform," *Appl. Sci.*, vol. 8, no. 11, p. 2167, Nov. 2018.

[18] Q. Tian et al., "New security mechanisms of high-reliability IoT communication based on radio frequency fingerprint," *IEEE Internet Things J.*, vol. 6, no. 5, pp. 7980–7987, Oct. 2019.

[19] F. Kandah, J. Cancelleri, D. Reising, A. Altarawneh, and A. Skjellum, "A hardware-software codesign approach to identity, trust, and resilience for IoT/CPS at scale," in *Proc. Int. Conf. Internet Things (iThings) IEEE Green Comput. Commun. (GreenCom) IEEE Cyber, Phys. Social Comput. (CPSCom) IEEE Smart Data (SmartData)*, Jul. 2019, pp. 1125–1134.

[20] G. Baldini, R. Giuliani, and C. Gentile, "An assessment of the impact of IQ imbalances on the physical layer authentication of IoT wireless devices," in *Proc. Global IoT Summit (GIoTS)*, Jun. 2019, pp. 1–6.

[21] F. J. Franco, I. Lopez-Calle, J. G. Izquierdo, and J. A. Agapito, "Modification of the LM124 single event transients by load resistors," *IEEE Trans. Nucl. Sci.*, vol. 57, no. 1, pp. 358–365, Feb. 2010.

[22] S. Buchner et al., "Comparison of single-event transients induced in an operational amplifier (LM124) by pulsed laser light and a broad beam of heavy ions," *IEEE Trans. Nucl. Sci.*, vol. 51, no. 5, pp. 2776–2781, Oct. 2004.

[23] S. Buchner and D. McMorrow, "Single-event transients in bipolar linear integrated circuits," *IEEE Trans. Nucl. Sci.*, vol. 53, no. 6, pp. 3079–3102, Dec. 2006.

[24] J. F. Ziegler, M. D. Ziegler, and J. P. Biersack, "SRIM—The stopping and range of ions in matter (2010)," *Nucl. Instrum. Methods Phys. Res. B, Beam Interact. Mater. At.*, vol. 268, nos. 11–12, pp. 1818–1823, Jun. 2010.

[25] E. W. Van Stryland et al., "Two photon absorption, nonlinear refraction, and optical limiting in semiconductors," *Opt. Eng.*, vol. 24, no. 4, pp. 613–623, Aug. 1985.

[26] T. Boggess, K. Bohnert, K. Mansour, S. Moss, I. Boyd, and A. Smirl, "Simultaneous measurement of the two-photon coefficient and free-carrier cross section above the bandgap of crystalline silicon," *IEEE J. Quantum Electron.*, vol. QE-22, no. 2, pp. 360–368, Feb. 1986.

[27] A. Khachatrian, N. J.-H. Roche, D. McMorrow, J. H. Warner, S. P. Buchner, and J. S. Melinger, "A dosimetry methodology for two-photon absorption induced single-event effects measurements," *IEEE Trans. Nucl. Sci.*, vol. 61, no. 6, pp. 3416–3423, Dec. 2014.